

Functional characterization of three mouse formyl peptide receptors

Hui-Qiong He, Dan Liao, Zhen-Guo Wang, Zhong-Li Wang, Hu-Chen Zhou, Ming-Wei Wang,

Richard D. Ye

School of Pharmacy, Shanghai Jiao Tong University, Shanghai, P.R. China (H.Q.H., D.L., Z.L.W.,
H.C.Z., R.D.Y.); Department of Pharmacology, College of Medicine, University of Illinois,
Chicago, Illinois (Z.G.W., R.D.Y.); The National Center for Drug Screening, Shanghai, P.R. China
(M.W.W.)

Running title: Functional characterization of three mouse Fprs

Correspondence: Richard D. Ye, School of Pharmacy, Shanghai Jiao Tong University, 800

Dongchuan Road, Shanghai, 200240, P.R. China. Tel. +86 21 34205430, Fax: +86 21 34204457;

E-mail: yedequan@sjtu.edu.cn

Number of text pages: 35

Number of tables: 3

Number of figures: 6

Number of References: 33

Number of words in Abstract: 213

Number of words in Introduction: 573

Number of words in Discussion: 1467

Abbreviations:

FPR, formyl peptide receptor; mFpr1, mouse formyl peptide receptor 1; mFpr2, mouse formyl

peptide receptor 2; mFpr-rs1, mouse formyl peptide receptor-related sequence 1; fMLF,

N-formyl-methionyl-leucyl-phenyl-alanine; WKYMVm, Trp-Lys-Tyr-Met-Val-D-Met; RBL, rat

basophilic leukemia; HBSS, Hanks's balanced saline solution; BSA, bovine serum albumin; FITC,

fluorescein isothiocyanate; EGFP, enhanced green fluorescent protein.

Abstract

The evolutionary relationship and functional correlation between human formyl peptide receptors (FPRs) and their mouse counterparts remain incompletely understood. We examined 3 members of the mouse formyl peptide receptor subfamily (mFprs) and found that they differ in agonist preference and cellular distributions. When stably expressed in transfected RBL-2H3 cells, mFpr1 was readily activated by *N*-formylated peptides derived from *Listeria monocytogenes* (fMIVTLF), *Staphylococcus aureus* (fMIFL) and mitochondria (fMMYALF). In contrast, the *Escherichia coli*-derived fMLF was 1,000-fold less potent. The above peptides were much less efficacious at mFpr2, which responded better to the synthetic hexapeptide WKYMVm, the synthetic agonists Quin-C1 (a substituted quinazolinone), and Compound 43 (a nitrosylated pyrazolone derivative). Saturation binding assays showed that mFpr1 and mFpr2 were expressed at similar levels on the cell surface, although their affinity for fMLFIK-FITC varied by more than 1,000-fold (K_d values of 2.8 nM for mFpr1 and 4.8 μ M for mFpr2). Contrary to these receptors, mFpr-rs1 responded poorly to all peptides tested above. Fluorescent microscopy revealed an intracellular distribution pattern of mFpr-rs1. Based on these results, we conclude that mFpr1 is an orthologue of human FPR1 with certain pharmacological properties of human FPR2/ALX, whereas mFpr2 has much lower affinity for formyl peptides. The intracellular distribution of mFpr-rs1 suggests an evolutionary correlation with human FPR3.

Introduction

The G-protein coupled formyl peptide receptors (FPRs) contribute to the migration of phagocytes to sites of infection and inflammation. The human FPR gene family has three identified members, *FPR1*, *FPR2*, and *FPR3*, which encode 3 distinct receptors (Migeotte et al., 2006; Rabiet et al., 2007; Ye et al., 2009). Among the 3 receptors, FPR1 and FPR2/ALX display high similarity (69%) in primary sequences. They also share several agonists including the synthetic hexapeptide WKYMVm (Trp-Lys-Tyr-Met-Val-D-Met-NH₂) and non-peptide molecules such as compound 43 (Forsman et al., 2011; Le et al., 1999). *N*-formylated peptides derived from bacteria or mitochondria are most potent chemoattractants for FPR1, triggering phagocytic activities including chemotaxis, calcium mobilization, degranulation and release of superoxide anions (Le et al., 2002). The tripeptide fMLF (*N*-formyl-Met-Leu-Phe) derived from *Escherichia coli* is the shortest high affinity agonist for FPR1. As for FPR2/ALX, other bacteria or mitochondria-derived formyl peptides are more potent agonists than fMLF (Rabiet et al., 2005). FPR3 responds poorly to formyl peptides except fMMYALF (*N*-formyl-Met-Met-Tyr-Ala-Leu-Phe), a hexapeptide derived from mitochondrial NADH dehydrogenase subunits 4, which displayed an EC₅₀ of 1×10⁻⁶ M in calcium mobilization assay (Rabiet et al., 2005). Of note, FPR2/ALX is a highly promiscuous receptor that can interact with agonists of various structures, including small proteins, peptides and synthetic molecules such as serum amyloid A (SAA), lipoxin A₄, as well as a substituted quinazolinone Quin-C1 (4-butoxy-N-[2-(4-methoxy-phenyl)-4-oxo-1,4-dihydro-2H-quinazolin-3-yl]-benzamide) (Chiang et al., 2006; He et al., 2003; Nanamori et al., 2004). In contrast, FPR3 has only a few high

affinity endogenous ligands including F2L, an acetylated amino-terminal peptide of the heme-binding protein (Migeotte et al., 2005). FPR3 has shown unique constitutive internalization (Rabiet et al., 2011) and its physiological function remains largely unknown.

The mouse *Fpr* gene family is more complex and contains at least 8 related genes, including *Fpr1*, *Fpr2*, *Fpr-rs1*, *Fpr-rs3*, *Fpr-rs4*, *Fpr-rs5*, *Fpr-rs6*, *Fpr-rs7* and *Fpr-rs8* (Gao et al., 1998; Tiffany et al., 2011; Ye et al., 2009). The first three genes code for receptors (mFpr1, mFpr2, and mFpr-rs1) that are found in leukocytes (Gao et al., 1999; Gao and Murphy, 1993; Hartt et al., 1999; Southgate et al., 2008). *Fpr1*^{-/-} neutrophils showed susceptibility to *Listeria* infection, suggesting that it has an important function in host defense against *Listeria* (Gao et al., 1999). mFpr1 was highly responsive to fMIFL (*N*-formyl-Met-Ile-Phe-Leu), while it showed low affinity binding of fMLF (Southgate et al., 2008). Moreover, its putative ligand binding domains resemble those of FPR2/ALX rather than FPR1. mFpr2 and mFpr-rs1 show sequence similarity to human FPR2/ALX and FPR3, respectively. It is presently unclear whether *Fpr-rs1* or *Fpr2* is the orthologue of FPR2/ALX, because both receptors are reported to respond to LXA4 (Takano et al., 1997; Vaughn et al., 2002). Additionally, mFpr2 has been found to be less responsive to fMIFL but serves as a receptor for F2L, a highly potent and specific agonist for human FPR3 (Gao et al., 2007; Southgate et al., 2008). These observations suggest that human FPRs, especially FPR1 and FPR3, have better defined and more specialized ligand-binding properties than the mouse receptors.

The present study was undertaken to clarify the functional and binding properties of selected mouse *Fpr* family members. Using RBL-2H3 cells stably transfected to express mFpr1, mFpr2 and mFpr-rs1, respectively, we compared the cellular response to formyl peptides and selected

synthetic agonists (Table 1). Saturation and competition binding assays were also performed with these agonists to further elucidate the pharmacological features of the mouse receptors.

Materials and Methods

Materials. WKYMVm and other peptides except fMLF used in this study were synthesized at Shanghai Science Peptide Biological Technology Co., LTD (Shanghai, China) and purified to $\geq 90\%$ homogeneity. *N*-formyl-Met-Leu-Phe-Ile-Ile-FITC was synthesized, conjugated and purified ($\geq 96\%$) at Shanghai Science Peptide Biological Technology Co., LTD. fMLF ($\geq 90\%$ purity) was purchased from Sigma-Aldrich (St. Louis, MO). Quin-C1 was synthesized as previously described (Nanamori et al., 2004; Zhou et al., 2007). Compound 43 was synthesized in-house according to the method described (Burli et al., 2006). FLIPR Calcium 5 reagent was obtained from Molecular Devices (Sunnyvale, CA). Other chemicals were purchased from Sigma-Aldrich.

Cell Culture. The rat basophilic leukemia cell line RBL-2H3 (ATCC, Manassas, VA) was transfected with an expression vector SFFV.neo containing the mFpr1, mFpr2 or mFPR-rs1 cDNA, as previously described (He et al., 2000). Stable transfectants were selected with 250 $\mu\text{g/ml}$ G418 (Invitrogen, Calsbad, CA) after initial isolation with 500 $\mu\text{g/ml}$ of G418. RBL stable cell lines were maintained at 37°C in 5% CO₂ in DMEM supplemented with 20% heat-inactivated FBS and 250 $\mu\text{g/ml}$ G418.

Degranulation. β -hexosaminidase release assay was performed as described (Nanamori et al., 2004). Briefly, RBL-2H3 cells (0.2×10^6 /well) expressing mFpr1, mFpr2 or mFpr-rs1 were seeded

in 24-well tissue culture plates for 24 h. After washing twice with HBSS-HB (20 mM HEPES in Hank's balanced salt solution with 0.5 mM CaCl₂ and 1 mM MgCl₂ supplemented with 0.1% BSA, PH 7.4), cells were pre-incubated with 10 μM cytochalasin B for 15 min on ice and 15 min at 37°C successively. Agonists were then applied at desired concentrations. The reaction was terminated after a 10-min stimulation by placing the plate on ice. β-hexosaminidase release into the medium was determined by incubating 20 μl of supernatant or cell lysate with 10 μl of 1 mM p-nitrophenyl-N-acetyl-β-D-glucosamide in 0.1 M sodium citrate buffer (pH 4.5) at 37°C for 1 h. At the end of the incubation, 200 μl of a 0.1 M Na₂CO₃/NaHCO₃ buffer (pH = 10) were added. Absorbance was monitored at 405 nm in a FlexStation III Spectrometer (Molecular Devices). Values (means ± SEM) were expressed as a percent of total β-hexosaminidase present in the cells.

Calcium Mobilization. Cells were grown to 90% confluence in black/clear bottom 96-well assay plates. The calcium mobilization assay was performed using Calcium 5 reagent according to manufacture's protocol. After 1 h incubation with the reagent (37°C, with 5% CO₂), the agonists were added robotically and samples were read in the FlexStation III with an excitation wavelength at 485 nm and an emission wavelength at 525 nm. Data were acquired by SoftMax® Pro 6 (Molecular Devices) and analyzed with Origin 7.5 software (Northampton, MA). The dose response curves were plotted as means ± SEM based on at least 3 experiments using 7-9 different concentrations of agonists.

Ligand binding assay. RBL stable transfectants were harvested, washed and resuspended at 1 × 10⁶/ml in extracellular buffer (HBSS plus 0.5 % BSA and 20 mM HEPES, PH 7.4) on ice. Binding assays were performed in Falcon™ polypropylene tubes (Becton Dickinson, Franklin

Lakes, NJ). For saturation binding assays, fMLFIK-FITC was used at concentrations from 10^{-10} to 10^{-5} M. Total binding and nonspecific binding were measured in the absence and presence of the unlabeled ligands in excess (50 μ M WKYMVm or 50 μ M fMLFIK, respectively). The cells were equilibrated for 1 h on ice and then analyzed for mean fluorescent intensity on a FACScan® flow cytometer (Becton Dickinson), with dead cells excluded by gating on forward and side scatter. The dissociation constant (K_d) was calculated for specific binding using one-site binding hyperbola nonlinear regression analysis as shown in the equation: $\text{Bound} = B_{\text{max}} \times [L] / ([L] + K_d)$, where B_{max} is the maximal number of binding sites, K_d is the concentration of labeled ligand (fMLFIK-FITC) required to reach half-maximal binding, and $[L]$ is the concentration of the labeled ligand. Receptor density was estimated with FITC-conjugated bead standards of known fluorescein equivalents (Quantum™ FITC-5 Premix, Lot #9975, Bangs Laboratories, Fishers, IN). A correction factor of 1.52 was used according to a previous study which showed the difference in fluorescence intensity between free fluorescein and peptide-conjugated FITC and the quenching upon binding to receptor (Vilven et al., 1998). The receptor number per cell was derived from an analysis of specific binding of fMLFIK-FITC at saturated concentrations. The relative affinities of the non-fluorescent ligands were measured in competitive binding assays, in which fMLFIK-FITC (50 nM for mFpr1-RBL cells or 5 μ M for mFpr2-RBL cells) was added on ice for 1 h prior to the addition of increasing concentrations of the competitors. Samples were incubated for another 1 h on ice, and competitive binding curves were obtained by flow cytometry. IC_{50} and Hill coefficient (n_H) values were calculated by fitting data points to the standard four-parameter logistic function, using nonlinear regression analysis with Origin 7.5. Experimentally determined

values are given as the means \pm SEM.

Receptor internalization. EGFP-tagged mFpr constructs were prepared by ligation of mFpr cDNAs to the N-terminus of EGFP coding sequence. RBL-2H3 cells were transfected to express individual mFpr-EGFP constructs, and stable transfectants were selected. N-terminal and C-terminal FLAG-tagged mFpr constructs were prepared and expressed in RBL-2H3 cells. FLAG-tagged mFpr-rs1 receptors were labeled with anti-FLAG monoclonal antibody (Sigma-Aldrich) for 1 h at room temperature. Cells were washed three times and incubated with green fluorescent Alexa 488-conjugated goat anti-rabbit antibody (Molecular Probes, Eugene, OR) for 30 min at room temperature. For internalization, HeLa cells were transiently transfected to express EGFP-tagged mFpr constructs with LipofectamineTM 2000 (Invitrogen, Carlsbad, CA). The transfected cells were grown on a glass cover slip for 24 h in DMEM supplemented with 10% FBS. The cells were washed briefly with HBSS-HB and stimulated with the testing agonists at 37°C for 30 min. Internalization was terminated by addition of fixation buffer (4% paraformaldehyde in PBS) followed by incubation at room temperature for 15 min. The cells were then washed twice with PBS and nuclei were stained by 4, 6-diamidino-2-phenylindole (DAPI, Beyotime, Shanghai) for 10 min at room temperature. Fluorescent images were taken on a Leica SP5 II inverted fluorescent confocal microscope.

Results

Agonists induced degranulation in RBL-2H3 cells expressing mFpr1, mFpr2 but not mFpr-rs1. To establish an agonist response profile for the mouse Fpr family, stable transfectants

expressing mFpr1 (NCBI: NP_038549.1), mFpr2 (NCBI: NP_032065.1) or mFpr-rs1 (NCBI: NP_032068.2) were stimulated with various FPR agonists including two synthetic small molecules (Quin-C1, Compound 43), a D-methionine-containing peptide (WKYMVm), and N-formylated peptides containing bacterial or mitochondrial protein sequences (Table 1). The release of β -hexosaminidase was measured and the results were compared with these agonists (Figure 1A, B and C). WKYMVm, Quin-C1 and Compound 43 activated both mFpr1 and mFpr2 with similar potency. In contrast, mFpr-rs1 hardly responded to any of the agonists tested except WKYMVm, which elicited granule release above 100 nM. Interestingly, in degranulation assays mFpr1 responded poorly to fMLF, and mFpr2 did not respond to fMLF up to 10 μ M. The poor response to fMLF prompted us to determine whether formyl peptides with different sequences could be better agonists for these mouse receptors. As shown in Figure 1D, all but fMLFK induced degranulation equal or better than fMLF at mFpr1, suggesting that peptide length and/or composition are factors that influence the response of this receptor. For instance, the tetrapeptides fMLFK, fMLFE, fMLFW and the pentapeptide fMLFII respectively showed 1.5, 3.6, 5.1 and 6.7-fold higher potency compared to fMLF when tested at 1 μ M. The formyl peptides derived from *S. aureus* (fMIFL), *L. monocytogenes* (fMIVTLF) and human mitochondria (fMMYALF) also had higher potency for mFpr1 (Figure 1D). In contrast, none of the 7 peptides tested was potent agonist for mFpr2, and only fMLFII and fMLFK could induce about 3.5 to 5% of β -hexosaminidase release through mFpr2, when used at 10 μ M (supplemental Figure 1C). These observations suggest that detection of N-formylated peptides may not be a primary function of mFpr2 and mFpr-rs1.

The three mFprs responded differently to agonists in calcium mobilization assays.

Agonists were further assayed for their ability to trigger calcium mobilization through activation of three chosen members of the mouse Fpr family. In Figure 2, representative tracings showing relative concentrations of intracellular Ca^{2+} were displayed in the upper panels and dose response curves were showed in the lower panels for the individual agonists tested. The untransfected RBL-2H3 cells did not respond to any one of the tested ligands, even when used at a high concentration of 10 μM . In comparison, the three receptor-expressing cell lines displayed varied responses to these agonists. The synthetic chemical Compound 43 preferentially activated mFpr1 over mFpr2 with a 10-fold higher potency (EC_{50} 187 nM vs. 1.2 μM ; Figure 2A and Table 2). Another synthetic compound, Quin-C1 (Figure 2B), was less potent than Compound 43, but its potency on mFpr1 and mFpr2 was similar. Based on the maximal calcium response as well as degranulation data, both Quin-C1 and Compound 43 are highly efficacious at these receptors. In fact, their efficacies are only surpassed by WKYMVm, which is highly efficacious for these receptors with an EC_{50} value of 82 pM for mFpr1 and 449 pM for mFpr2 (supplemental Figure 2A).

Among the native agonists tested, fMMYALF (mitochondria) and fMIVTLF (*L. monocytogenes*) had the highest potency for mFpr1 (EC_{50} = 21 and 98 pM), and they triggered intracellular Ca^{2+} flux even more efficaciously than WKYMVm (Figure 2C and 2D). As previously reported (Southgate et al., 2008), the *S. aureus*-derived fMIFL stimulated marked Ca^{2+} increase in mFpr1-RBL cells with an EC_{50} in the high picomolar range (350 pM, Supplemental

Figure 2C). fMLFII and fMLFIIK, both derived from fMLFI (*S. aureus*) with C-terminal extensions, showed similar potency on mFpr1-RBL cells in calcium mobilization assays (EC_{50} 310 and 460 pM, respectively; Figure 2H and Supplemental Figure 2D). In agreement with previous findings (Southgate et al., 2008), mFpr1 preferred these bacterial and mitochondrial formyl peptides over *E. coli*-derived fMLF (EC_{50} = 23 μ M, Supplemental Figure 2B), fMLFK (EC_{50} = 510 nM), fMLFE (EC_{50} = 6.7 nM) and fMLFW (EC_{50} = 1.1 nM) (Figure 2E-G and Table 2).

In contrast to mFpr1, mFpr2 responded poorly to all the formyl peptides tested. The hexapeptides fMIVTLF and fMMYALF had EC_{50} values of 2.8 μ M and 4.7 μ M in calcium flux assays, respectively. The other two peptides, fMLFII (Figure 2H) and fMLFIIK (Supplemental Figure 2D), exhibited somewhat higher potency, with EC_{50} of 910 nM and 900 nM, respectively. The tetrapeptides fMLFW and fMLFK were less potent at mFpr2, with EC_{50} values in micromolar range (3.3 and 2.3 μ M, Figure 2E and 2G). While fMIFL was active on mFpr2 only above 10 μ M (EC_{50} = 53 μ M), the *E. coli* derived peptide fMLF (Supplemental Figure 2B) and its longer derivative fMLFE (Figure 2F) were essentially inactive at mFpr2.

Throughout these experiments, the mFpr-1-RBL cells were insensitive to all agonists except WKYMVm, which induced calcium flux at a very high concentration (supplemental Figure 2A). Because of the variability, we next examined cellular distribution of the receptors in transfected RBL cells.

The cellular distribution profile of mFpr-rs1 differs from that of mFpr1 and mFpr2. To determine whether the mouse receptors are expressed on cell surface, the green fluorescent protein EGFP was fused to the C-terminus of the mouse Fpr proteins. The resulting chimeric receptors

were either expressed in RBL cells for selection of stable transfectants, or transiently expressed in HeLa cells. Like human FPR1 and FPR2/ALX, mFpr1-EGFP and mFpr2-EGFP chimeric receptors were found mostly on cell surface in the transfected RBL-2H3 cells (Figure 3A and 3B) and HeLa cells (Figure 3E and 3F). Moreover, mFpr1-EGFP and mFpr2-EGFP internalized upon agonist stimulation in HeLa cells (Figure 3G to 3N). The level of internalization correlates approximately with the potency of the agonist as measured in parallel degranulation and calcium mobilization assays.

In contrast, mFpr-rs1-EGFP showed a more uniform cellular distribution profile. This pattern remained unchanged when expressed in RBL-2H3 (Figure 3C and 3D), HeLa cells (Supplemental Figure 3) and HEK293 cells (data not shown). To exclude the possibility that the minimal cell surface expression might result from unwanted frame shift or early transcription termination, full-length sequencing was performed and a normal reading frame was confirmed. Additional mFpr-rs1 expression plasmids were constructed by tagging the receptor with a much smaller FLAG sequence (N-DYKDDDDK-C) to either the N- or C-terminus of mFpr-rs1. HeLa cells were transfected to express mFpr-rs1-N-FLAG or mFpr-rs1-C-FLAG. Thirty-six hours after transfection, cells were incubated with an anti-FLAG antibody and labeled with Alexa Fluoro 488-conjugated secondary antibody. The mFpr-rs1-N-FLAG and mFpr-rs1-C-FLAG receptors were mostly visualized inside the cells (Supplemental Figure 3), suggesting that the expression pattern of mFpr-rs1 receptor did not change inadvertently because of the addition of an EGFP.

The mouse formyl peptide receptors have distinct patterns of agonist binding. To determine the binding affinity of the three mouse receptors, a FITC-conjugated fMLFIK was

synthesized and saturation binding assays were performed using flow cytometry (*Materials and Methods*). The untransfected RBL cells produced little background binding to the fluorescent ligand (data not shown). Unlike radiolabeled ligands, nonspecific binding was relatively low with the FITC-conjugated fMLFIIK (Figure 4A). A dissociation constant (K_d) of 2.8 ± 0.4 nM and a binding capacity (B_{max}) of $90,468 \pm 7,805$ binding sites per cell were derived for the mFpr1-RBL cells. Scatchard plot (inset) and Hill plot (not shown) confirmed a one-site binding model. In contrast, total binding to either mFpr2 or mFpr-rs1 were low, thus no significant specific binding were measurable within the same nanomolar concentration range of fMLFIIK-FITC (0 - 100 nM) as with the mFpr1-RBL cells. However, an increase in ligand binding to mFpr2 or mFpr-rs1 was detected in the micromolar concentration range, which approached saturation at 10 μ M or above, despite a high background caused by nonspecific binding (Figure 4B and 4C). The estimated K_d values based on these experiments were 4.8 ± 0.2 and 6.2 ± 0.3 μ M respectively, suggesting low-affinity binding for fMLFIIK to mFpr2 and mFpr-rs1. The number of total binding sites was estimated with 7 μ M fMLFIIK-FITC, using FITC-conjugated standard beads as reference. The results suggested that approximately 100,000 mFpr2 was expressed in the transfected RBL cells, which is slightly more than the expression of mFpr1 (data not shown). In contrast, only 5,000 to 9,000 mFpr-rs1 were found on the surface of transfected RBL cells, which is about 10% of the numbers of mFpr1 and mFpr2 in the transfected RBL cells. This observation is consistent with the results from fluorescent microscopy (Figure 3C, 3D) and support the notion that a significant portion of mFpr1-rs1 is present inside the cells.

To compare the pharmacological properties of agonists from a variety of sources, competitive

binding assays were performed using RBL cells stably expressing mFpr1 with a fixed amount of fMLFIIK-FITC (50 nM) and variable concentrations of unlabeled agonists (Figure 5A). Table 3 summarized the IC_{50} values of these competitive ligands. Among the agonists tested, fMLFII showed the highest potency to displace fMLFIIK-FITC from mFpr1-RBL cells ($IC_{50} = 5.4$ nM). An extended version of this peptide, fMLFIIK, displayed a 40-fold less potency ($IC_{50} = 216$ nM). Consistent with the results from functional assays, WKYMVm and fMIVTLF were also strong competitors of fMLFIIK (IC_{50} values of 11.7 nM and 24.4 nM), while fMLFW, fMMYALF and fMIFL displaced fMLFIIK-FITC with lower potency ($IC_{50} = 153$ nM, 272 nM and 415 nM). The synthetic chemicals Compound 43 and Quin-C1 were weaker competitors ($IC_{50} = 7.8$ μ M and 8.5 μ M, respectively) despite their agonistic activities in functional assays. This may result from the fact that peptides and the chemicals occupy binding sites that are only partially overlapping. Finally, fMLF and fMLFK showed inability to cause any displacement below 10 μ M ($IC_{50} = 46.6$ and 405 μ M, Figure 5 and Table 3).

Since mFpr2 binds fMLFIIK-FITC with lower affinity than mFpr1, a concentration of 5 μ M was used in competition binding assays (Figure 5B). Table 3 showed that the IC_{50} values for mFpr2-RBL cells were at least 1~2 orders of magnitude larger than those for mFpr1-RBL cells. WKYMVm was the strongest competitor ($IC_{50} = 708$ nM), though it induced incomplete displacement (<80%) of fMLFIIK-FITC, suggesting that its binding site partially overlaps with the site for formyl peptides on mFpr2. Quin-C1 was 4.5-fold more potent than Compound 43, with the respective IC_{50} values of 137 μ M and 610 μ M. The peptides fMLFII, fMIVTLF and fMLFIIK displaced fMLFIIK-FITC from mFpr2 with micromolar concentrations ($IC_{50} = 3.8$, 4.7 and 6.4

μM , respectively). In comparison, fMLF, fMLFE, fMLFW, fMIFL and fMMYALF were incapable of displacing fMLFIK-FITC, while fMLFK at very high concentrations ($>50 \mu\text{M}$) showed limited potency in competition binding assay (Table 3, Figure 5B). In addition, as expected, the nonformylated peptide MLFIK caused no displacement on either mFpr1-RBL or mFpr2-RBL cells (Figure 6), suggesting that the N-formyl group is essential for the peptide fMLFIK to bind mFpr1 and mFpr2. We were unable to perform meaningful competitive binding assays on mFpr-rs1 due to the limited cell surface expression and low affinity for the agonist.

Discussion

So far, most functional studies of the FPRs have been conducted in human neutrophils and some early studies were conducted using rabbit neutrophils. In comparison, much less is known about the FPRs from other species. In mice, the number of genes coding for putative Fpr family receptors far exceeds that in humans. Although there are 8 members in the mouse *Fpr* gene family, not all of them have been identified to encode formyl peptide receptors. For instance, *Fpr-rs5* (Ψ *Fpr-rs3*) is a pseudogene and *Fpr-rs8* (Ψ *Fpr-rs2*) has been recently characterized as a constitutively expressed gene that may affect longevity (Tiffany et al., 2011). mFpr-rs 3, 4, 6 and 7 were reported to be expressed by vomeronasal sensory neurons and function as chemoreceptors (Liberles et al., 2009; Riviere et al., 2009). The remaining 3 genes (*Fpr1*, *Fpr2* and *Fpr-rs1*), which are expressed in mouse phagocytic leukocytes, are most similar to human FPRs at protein sequence level. Generally, they have been considered to be the orthologues of human *FPR* members. However, the promiscuous binding property of these 3 receptors and complex

evolutionary relationship make it difficult to accurately define orthologous correlation between members of the human and mouse formyl peptide receptor gene families. With rapid advancement in mouse genetics that has already helped to unveil the functional roles played by selected Fprs (Chen et al., 2010; Dufton et al., 2010; Gao et al., 1999), it will be possible to use mouse Fpr as models for study of human diseases. Therefore, it is important to gain a better understanding of the pharmacological properties of the mouse Fpr family members.

The 3 mFpr family members studied in this work exhibit high sequence homology to the human FPRs, and their tissue distribution profile also resembles that of the human FPRs. It has been suggested that, despite being closest (76%) in primary sequence to hFPR1, mFPR1 shares several features found in human FPR2/ALX. For example, both mFpr1 and human FPR2/ALX are low-affinity receptors for the *E. coli*-derived fMLF, while they respond well to formyl peptides derived from *S. aureus* (fMIFL), *L. monocytogenes* (fMIVTLF) and mitochondria (fMMYALF) (Rabiet et al., 2005; Southgate et al., 2008). It should be noted that while fMLF is a major chemotactic peptide in *E. coli* culture supernatant, it is not the only one that stimulates neutrophil response. In this work, we found that mFpr1 displays higher affinity for fMLF derivatives in the order of fMLFW > fMLFE > fMLFK > fMLF. This observation indicates that, besides the N-formylated group, the addition of amino acids to the C-terminus of formyl peptides may promote binding to mFpr1. There is also evidence that longer peptides such as fMLFII and fMLFIIK often behave better in functional and binding assays.

The second mouse receptor, mFpr2, is believed to be a low-affinity receptor for formyl peptides (Hartt et al., 1999). It has a more restricted specificity for the peptides tested in this work,

but responds better to non-peptides such as Quin-C1 and Compound 43. Besides, mFpr2 responds well to WKYMVm, a peptide that contains a D-methionine. These findings suggest that the native ligands for mFpr2 may not be formylated peptides. Studies have shown that some of the mouse Fprs, including mFpr2 and mFpr-rs1, are receptors for lipoxin A4 (Takano et al., 1997; Vaughn et al., 2002). Recent knockout studies have shown that mFpr2 plays an important role in airway inflammation and immune response (Chen et al., 2010). Hence, a more detailed characterization of this receptor is of potential interest as it may provide a useful animal model for study of human lung diseases. Regardless of its low affinity for fMLF, mFpr2 retains some capability in binding formyl peptides. Longer formyl peptides such as fMLFK, fMLFII, and fMLFIHK are better agonists for this receptor. The relatively low efficacy and affinity of fMMYALF, fMIVTLF and fMIFL at mFpr2 suggests that the sequence as well as side chains of C-terminal residues in these peptides can be more crucial than the length for binding to mFpr2.

Sequence comparison has shown similarities and differences between the mouse and human FPRs and between the 3 mouse Fprs tested in this study. Notably, some important residues such as Arg205, known to be critical for the interaction with formylated peptides at their C-terminus (Mills et al., 2000), are not present in all receptors. In human FPR3, A histidine takes place at position 205, but whether this substitution is sufficient to alter ligand binding specificity remains unclear because an arginine is found at the same position in all 3 mFprs tested. Likewise, residues at positions 83 - 85 and 284 (based on the human FPR1 sequence), known to be involved in binding of formyl peptides (Lala et al., 1999; Mills et al., 1998; Quehenberger et al., 1997), are substituted to various degrees in the human FPRs and mouse Fprs tested so far. These observations pose

challenges to sequence-based modeling as well as structure-function studies relying on site-directed mutagenesis. The complexity and diversity of ligands for the FPR family provides an excellent model to study GPCR structures and functions.

In this study, we found that Quin-C1, a substituted quinazolinone, activated both mFpr2 and mFpr1 with almost equal potency in calcium flux assay. Compound 43, a nitrosylated pyrazolone derivative, was 100-fold more potent at mFpr1 in functional and binding assays. These findings are in agreement with a previous study by Dahlgren and colleagues that predicted shared binding between mFpr1 and mFpr2 for Compound 43 (Forsman et al., 2011). The synthetic small molecules are clearly different than formyl peptides in terms of binding site selection on the receptors. As we have shown in this study, Quin-C1 and Compound 43 are less effective in competing with fMLFIK-FITC for binding to the two receptors, despite their relatively high potency in functional assays. We have previously shown that Quin-C1 could not effectively displace radiolabeled WKYMVm in human FPR2/ALX binding assay, suggesting that their binding sites are only partially overlapping (Nanamori et al., 2004). It will be interesting to further investigate whether these synthetic molecules influence FPR family receptors through allosteric modulation.

The third mouse receptor studied, mFpr-rs1, shares similar structural features with mFpr2 and mFpr1 but differs from them with its unique intracellular distribution profile. Unlike mFpr1 and mFpr2, which are found mostly on cell surface, mFpr-rs1 was hardly detectable on plasma membrane in transfected RBL-2H3, HeLa and HEK293 cells. Instead, it was mostly visualized inside the transfected cells. The observed intracellular distribution in this work was not due to

artifact. In fact, the human FPR3 has the propensity of intracellular localization, as observed in blood monocytes (Migeotte et al., 2005). A possible mechanism for the intracellular localization of human FPR3 was reported recently (Rabiet et al., 2011). Therefore, mFpr-rs1 resembles human FPR3 in cellular distribution. The weak cell response to agonists found in this study might be attributable to its low expression on cell surface. Interestingly, peptides such as F2L, which is derived from the heme-binding protein (Migeotte et al., 2005), probably act through binding to a cell surface receptor. Whether there are additional and possibly intracellular agonists for mFpr-rs1 and human FPR3 remains an interesting question. Such agonists might be lipophilic and can permeate cell membrane to gain access to the intracellular pool of receptors. It is also possible that an agonist might recruit mFpr-rs1 from cytoplasm to the plasma membrane upon binding to the available receptors, resulting in an enrichment of cell surface receptors. However, none of the agonists tested in this work seem to possess this property.

In conclusion, we examined the pharmacological properties of 3 mFpr family members in transfected cells. Our results show that mFpr1 is an orthologue of the human FPR1, and both are high affinity receptors for N-formyl peptides. Major differences between these two receptors are that mFpr1 displays relatively low affinity for fMLF, and that it responds well to the synthetic molecule Quin-C1 whereas the human FPR1 does not (Nanamori et al., 2004). mFpr1 shares the latter property with human FPR2/ALX. Our results also show that, in general, formyl peptides are weak agonists for mFpr2, suggesting that its native ligand may not be a formylated peptide. Finally, we report for the first time that mFpr-rs1 has limited cell surface expression, a property shared with the human FPR3. Therefore, mFpr-rs1 may be an orthologue of human FPR3. In this regard, the

term mFpr3 is appropriate, although the natural ligand for the intracellular receptors remains to be determined. A ligand for human FPR3, F2L, has been shown to activate mFpr2, suggesting an overlapping feature of mFpr2 and human FPR3 (Gao et al., 2007). Intracellular GPCRs are rare, and their functions as well as signaling mechanisms are poorly understood. It is hopeful that a better understanding of the mouse Fpr family will facilitate the use of genetics tools for study of human FPR and their pathophysiological functions.

Acknowledgments

The authors would like to thank Dr. Erica Troksa and Dr. Masakatsu Nanamori for preparation of peptides.

Authorship contributions

Participated in research design: He and Ye.

Conducted experiments: He and Liao.

Contributed new reagents or analytic tools: Z.G. Wang, Z.L. Wang, Zhou and M.W. Wang.

Performed data analysis: He, Liao and Ye.

Wrote or contributed to the writing of the manuscript: He and Ye.

References

- Burli RW, Xu H, Zou X, Muller K, Golden J, Frohn M, Adlam M, Plant MH, Wong M, McElvain M, Regal K, Viswanadhan VN, Tagari P and Hungate R (2006) Potent hFPRL1 (ALXR) agonists as potential anti-inflammatory agents. *Bioorg Med Chem Lett* 16:3713-8.
- Chen K, Le Y, Liu Y, Gong W, Ying G, Huang J, Yoshimura T, Tessarollo L and Wang JM (2010) A critical role for the g protein-coupled receptor mFPR2 in airway inflammation and immune responses. *J Immunol* 184:3331-5.
- Chiang N, Serhan CN, Dahlen SE, Drazen JM, Hay DW, Rovati GE, Shimizu T, Yokomizo T and Brink C (2006) The lipoxin receptor ALX: potent ligand-specific and stereoselective actions in vivo. *Pharmacol Rev* 58:463-87.
- Dufton N, Hannon R, Brancalone V, Dalli J, Patel HB, Gray M, D'Acquisto F, Buckingham JC, Perretti M and Flower RJ (2010) Anti-inflammatory role of the murine formyl-peptide receptor 2: ligand-specific effects on leukocyte responses and experimental inflammation. *J Immunol* 184:2611-9.
- Forsman H, Onnheim K, Andreasson E and Dahlgren C (2011) What formyl peptide receptors, if any, are triggered by compound 43 and lipoxin A4? *Scand J Immunol* 74:227-34.
- Gao JL, Chen H, Filie JD, Kozak CA and Murphy PM (1998) Differential expansion of the N-formylpeptide receptor gene cluster in human and mouse. *Genomics* 51:270-6.
- Gao JL, Guillabert A, Hu J, Le Y, Urizar E, Seligman E, Fang KJ, Yuan X, Imbault V, Communi D, Wang JM, Parmentier M, Murphy PM and Migeotte I (2007) F2L, a peptide derived from heme-binding protein, chemoattracts mouse neutrophils by specifically activating Fpr2, the

- low-affinity N-formylpeptide receptor. *J Immunol* 178:1450-6.
- Gao JL, Lee EJ and Murphy PM (1999) Impaired antibacterial host defense in mice lacking the N-formylpeptide receptor. *J Exp Med* 189:657-62.
- Gao LJ and Murphy PM (1993) Species and subtype variants of the N-formyl peptide chemotactic receptor reveal multiple important functional domains. *J Biol Chem.* 268:25395-25401.
- Hartt JK, Barish G, Murphy PM and Gao JL (1999) N-formylpeptides induce two distinct concentration optima for mouse neutrophil chemotaxis by differential interaction with two N-formylpeptide receptor (FPR) subtypes. Molecular characterization of FPR2, a second mouse neutrophil FPR. *J Exp Med* 190:741-7.
- He R, Sang H and Ye RD (2003) Serum amyloid A induces IL-8 secretion through a G protein-coupled receptor, FPRL1/LXA4R. *Blood* 101:1572-81.
- He R, Tan L, Browning DD, Wang JM and Ye RD (2000) The synthetic peptide Trp-Lys-Tyr-Met-Val-D-Met is a potent chemotactic agonist for mouse formyl peptide receptor. *J Immunol* 165:4598-605.
- Lala A, Gwinn M and De Nardin E (1999) Human formyl peptide receptor function role of conserved and nonconserved charged residues. *Eur J Biochem* 264:495-9.
- Le Y, Gong W, Li B, Dunlop NM, Shen W, Su SB, Ye RD and Wang JM (1999) Utilization of two seven-transmembrane, G protein-coupled receptors, formyl peptide receptor-like 1 and formyl peptide receptor, by the synthetic hexapeptide WKYVM for human phagocyte activation. *J Immunol* 163:6777-84.

- Le Y, Murphy PM and Wang JM (2002) Formyl-peptide receptors revisited. *Trends Immunol* 23:541-8.
- Liberles SD, Horowitz LF, Kuang D, Contos JJ, Wilson KL, Siltberg-Liberles J, Liberles DA and Buck LB (2009) Formyl peptide receptors are candidate chemosensory receptors in the vomeronasal organ. *Proc Natl Acad Sci U S A* 106:9842-7.
- Migeotte I, Communi D and Parmentier M (2006) Formyl peptide receptors: a promiscuous subfamily of G protein-coupled receptors controlling immune responses. *Cytokine Growth Factor Rev* 17:501-19.
- Migeotte I, Riboldi E, Franssen JD, Gregoire F, Loison C, Wittamer V, Detheux M, Robberecht P, Costagliola S, Vassart G, Sozzani S, Parmentier M and Communi D (2005) Identification and characterization of an endogenous chemotactic ligand specific for FPRL2. *J Exp Med* 201:83-93.
- Mills JS, Miettinen HM, Barnidge D, Vlases MJ, Wimer-Mackin S, Dratz EA, Sunner J and Jesaitis AJ (1998) Identification of a ligand binding site in the human neutrophil formyl peptide receptor using a site-specific fluorescent photoaffinity label and mass spectrometry. *J Biol Chem* 273:10428-35.
- Mills JS, Miettinen HM, Cummings D and Jesaitis AJ (2000) Characterization of the binding site on the formyl peptide receptor using three receptor mutants and analogs of Met-Leu-Phe and Met-Met-Trp-Leu-Leu. *J Biol Chem* 275:39012-7.
- Nanamori M, Cheng X, Mei J, Sang H, Xuan Y, Zhou C, Wang MW and Ye RD (2004) A novel nonpeptide ligand for formyl peptide receptor-like 1. *Mol Pharmacol* 66:1213-22.

Quehenberger O, Pan ZK, Prossnitz ER, Cavanagh SL, Cochrane CG and Ye RD (1997)

Identification of an N-formyl peptide receptor ligand binding domain by a gain-of-function approach. *Biochem Biophys Res Commun* 238:377-81.

Rabiet MJ, Huet E and Boulay F (2005) Human mitochondria-derived N-formylated peptides are novel agonists equally active on FPR and FPRL1, while *Listeria monocytogenes*-derived peptides preferentially activate FPR. *Eur J Immunol* 35:2486-95.

Rabiet MJ, Huet E and Boulay F (2007) The N-formyl peptide receptors and the anaphylatoxin C5a receptors: an overview. *Biochimie* 89:1089-106.

Rabiet MJ, Macari L, Dahlgren C and Boulay F (2011) N-formyl peptide receptor 3 (FPR3) departs from the homologous FPR2/ALX receptor with regard to the major processes governing chemoattractant receptor regulation, expression at the cell surface, and phosphorylation. *J Biol Chem* 286:26718-31.

Riviere S, Challet L, Fluegge D, Spehr M and Rodriguez I (2009) Formyl peptide receptor-like proteins are a novel family of vomeronasal chemosensors. *Nature* 459:574-7.

Southgate EL, He RL, Gao JL, Murphy PM, Nanamori M and Ye RD (2008) Identification of formyl peptides from *Listeria monocytogenes* and *Staphylococcus aureus* as potent chemoattractants for mouse neutrophils. *J Immunol* 181:1429-37.

Takano T, Fiore S, Maddox JF, Brady HR, Petasis NA and Serhan CN (1997) Aspirin-triggered 15-epi-lipoxin A4 (LXA4) and LXA4 stable analogues are potent inhibitors of acute inflammation: evidence for anti-inflammatory receptors. *J Exp Med* 185:1693-704.

Tiffany HL, Gao JL, Roffe E, Sechler JM and Murphy PM (2011) Characterization of Fpr-rs8, an

atypical member of the mouse formyl peptide receptor gene family. *J Innate Immun* 3:519-29.

Vaughn MW, Proske RJ and Haviland DL (2002) Identification, cloning, and functional

characterization of a murine lipoxin A4 receptor homologue gene. *J Immunol* 169:3363-9.

Vilven JC, Domalewski M, Prossnitz ER, Ye RD, Muthukumaraswamy N, Harris RB, Freer RJ

and Sklar LA (1998) Strategies for positioning fluorescent probes and crosslinkers on formyl peptide ligands. *J Recept Signal Transduct Res* 18:187-221.

Ye RD, Boulay F, Wang JM, Dahlgren C, Gerard C, Parmentier M, Serhan CN and Murphy PM

(2009) International Union of Basic and Clinical Pharmacology. LXXIII. Nomenclature for the formyl peptide receptor (FPR) family. *Pharmacol Rev* 61:119-61.

Zhou C, Zhang S, Nanamori M, Zhang Y, Liu Q, Li N, Sun M, Tian J, Ye PP, Cheng N, Ye RD and

Wang MW (2007) Pharmacological characterization of a novel nonpeptide antagonist for formyl peptide receptor-like 1. *Mol Pharmacol* 72:976-83.

Footnotes

This work was supported in part by National Basic Research Program of China (973 Program)

[Grant 2012CB518001]. H.Q.H. is a recipient of Chinese Postdoctoral Science Fund

[Grant12Z102060002].

Request for reprints should be sent to: Richard D. Ye, School of Pharmacy, Shanghai Jiao Tong

University, 800 Dongchuan Road, Shanghai, 200240, P.R. China. E-mail: yedequan@sjtu.edu.cn

Figure legends

Figure 1. Degranulation induced by agonists through mFpr1, mFpr2 or mFpr-rs1 receptors. Release of β -hexosaminidase by fMLF, WKYMVm, Quin-C1 and Compound 43 at indicated concentrations were measured in RBL cells expressing mFpr1 (A), mFpr2 (B) or mFpr-rs1 (C) respectively. Various formyl peptides (1 μ M) were compared for the induction of β -hexosaminidase secretion (D). Values are mean \pm S.E.M. of single duplicate determinations and representative of at least three separate experiments.

Figure 2. Calcium mobilization in RBL-mFpr cells stimulated with various agonists. Cells were loaded with FLIPR Calcium 5 reagent and analyzed for changes of intracellular calcium in response to agonist stimulation. (A) Quin-C1, (B) Compound 43, (C) fMMYALF, (D) fMIVTLF, (E) fMLFK, (F) fMLFE, (G) fMLFW, (H) fMLFII. The upper panels show typical calcium traces in response to the indicated agonist concentration. The lower panels are dose-dependent curves, which were based on peak Ca^{2+} increase at indicated agonist concentrations and shown as mean \pm S.E.M. representing > 3 separate experiments.

Figure 3. Cell surface expression and internalization of mouse Fpr receptors. A-D, mFpr1-EGFP (A), mFpr2-EGFP (B), or mFpr-rs1-EGFP (C and D) expressed in RBL cells. The scale bar for A-C is shown in figure A and the images were captured using a 63 \times oil immersion objective, while the image of figure D was captured under a 40 \times dry objective and the scale bar is shown in the figure. E-N: internalization of mFpr1-EGFP or mFpr2-EGFP in HeLa cells, before (E and F) and after 30-minute stimulation, with fMLF (G and H), fMLFK (I and J), WKYMVm (K and L), Quin-C1 (M and N) or Compound 43 (O and P), at indicated concentrations. The scale bar

for E-P is shown in figure E and the images were captured using a 63× oil immersion objective.

Figure 4. Binding assays with RBL-2H3 cells stably transfected by mFpr1, mFpr2 or mFpr-rs1. A-C, Saturation, nonspecific and specific binding of fMLFIIK-FITC to mFpr1- (A), mFpr2- (B) or mFpr-rs1- (C) expressing RBL cells. The inset shows Scatchard analysis of the data in (A). Data were analyzed with Origin 7.5 software and the results are shown as means ± S.E.M. with > 3 experiments.

Figure 5. Competition binding assays performed on (A) mFpr1-RBL and (B) mFpr2-RBL cells. Binding of fMLFIIK-FITC (50 nM for mFpr1-RBL and 5 μM for mFpr2-RBL cells) was competitively displaced by increasing concentrations of agonists, including left panels, synthetic ligands WKYMVm, Quin-C1, Compound 43, middle panels, *E. Coli*-derived fMLF, derivatives fMLFK, fMLFE, fMLFW, fMLFII; and right panels, other bacterial formyl peptides fMIFL, fMIVTLF, and mitochondrial fMMYALF. Data were analyzed as described in the legend for Figure 4. The results are shown as means ± S.E.M. with > 3 experiments.

Figure 6. Comparison of formyl and nonformyl peptides in competitive binding assay. The ability of nonformylated peptide MLFIIK and *N*-formylated fMLFIIK to compete with fMLFIIK-FITC for binding to (A) mFpr1- and (B) mFpr2-RBL cells was determined. All data were analyzed as described in the legend of Figure. 4.

Table 1. The various agonists used in this study.

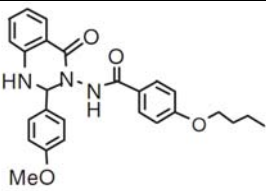
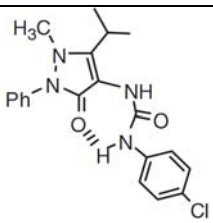
Sequence/Name	Origin
Formyl-MLF	<i>Escherichia coli</i>
Formyl-MLFK	Derivative of fMLF
Formyl-MLFE	Derivative of fMLF
Formyl-MLFW	Derivative of fMLF
Formyl-MIFL	<i>Staphylococcus aureus</i>
Formyl-MLFII	Derivative of fMIFL
Formyl-MLFIIK	Derivative of fMIFL
Formyl-MIVTLF	<i>Listeria monocytogenes</i>
Formyl-MMYALF	Mitochondria ND6 protein
WKYMVm	Peptide library screen
Quin-C1 	Small compound library screen
Compound 43 	Small compound library screen

Table 2. Calcium mobilization in RBL cells expressing mFpr1 or mFpr2 are induced by various agonists in a concentration-dependent manner. The EC₅₀ values and the maximum effects (relative Ca²⁺ flux) are shown below, based on > 3 independent experiments.

Agonists	mFpr1		mFpr2	
	EC ₅₀ (M)	MaxE	EC ₅₀ (M)	MaxE
fMLF	2.3 ± (2.7) × 10 ⁻⁵	2.6 ± 0.2	ND	ND
fMLFE	6.7 ± (1.1) × 10 ⁻⁹	3.6 ± 0.4	ND	ND
fMLFK	5.1 ± (1.0) × 10 ⁻⁷	3.6 ± 0.3	2.3 ± (.67) × 10 ⁻⁶	3.0 ± 0.3
fMLFW	1.1 ± (.16) × 10 ⁻⁹	4.6 ± 0.3	3.3 ± (.45) × 10 ⁻⁶	3.1 ± 0.3
fMIFL	3.5 ± (.46) × 10 ⁻¹⁰	4.8 ± 0.4	5.3 ± (2.6) × 10 ⁻⁴	1.7 ± 0.2
fMLFII	3.1 ± (.32) × 10 ⁻¹¹	4.8 ± 0.3	9.1 ± (3.7) × 10 ⁻⁷	3.3 ± 0.2
fMLFIK	4.6 ± (1.1) × 10 ⁻¹⁰	3.4 ± 0.1	9.0 ± (7.4) × 10 ⁻⁷	3.7 ± 0.1
fMIVTLF	2.1 ± (.45) × 10 ⁻¹¹	4.7 ± 0.4	2.8 ± (.55) × 10 ⁻⁶	2.6 ± 0.1
fMMYALF	9.8 ± (4.2) × 10 ⁻¹¹	4.1 ± 0.2	4.7 ± (3.1) × 10 ⁻⁶	2.4 ± 0.4
WKYMVm	8.2 ± (1.9) × 10 ⁻¹¹	4.6 ± 0.3	4.5 ± (1.2) × 10 ⁻¹⁰	4.0 ± 0.2
Quin C1	2.4 ± (.33) × 10 ⁻⁶	4.4 ± 0.2	6.3 ± (.92) × 10 ⁻⁷	3.6 ± 0.3
Compound 43	1.9 ± (.25) × 10 ⁻⁹	4.4 ± 0.4	1.2 ± (.17) × 10 ⁻⁷	3.0 ± 0.3

ND, not determined.

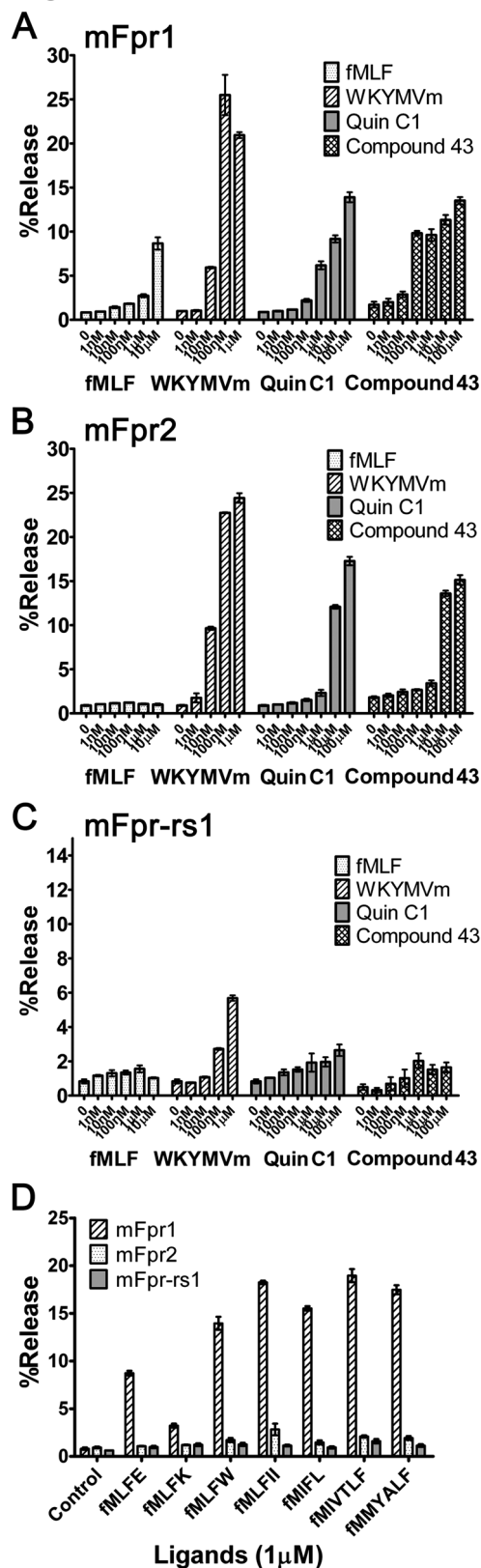
Table 3. Various agonists displacing fMLFIIK-FITC binding to mFpr1-RBL or mFpr2-RBL

cells with different affinity. Shown are the means of IC₅₀ values and Hill coefficient (n_H) of unlabeled ligands in competition binding assays conducted with at least 3 independent experiments as described.

Agonist	mFpr1-RBL		mFpr2-RBL	
	IC ₅₀ (M)	n _H	IC ₅₀ (M)	n _H
WKYMVm	1.2 ± (.06) × 10 ⁻⁸	1.2 ± 0.1	7.1 ± (1.6) × 10 ⁻⁷	0.6 ± 0.1
fMLF	4.7 ± (.98) × 10 ⁻⁵	1.0 ± 0.1	ND	ND
fMLFK	4.1 ± (.17) × 10 ⁻⁴	1.1 ± 0.5	> 5.6 × 10 ⁻⁵	ND
fMLFE	8.8 ± (1.1) × 10 ⁻⁶	0.6 ± 0.1	ND	ND
fMLFW	1.5 ± (.05) × 10 ⁻⁷	0.9 ± 0.03	ND	ND
fMLFII	5.4 ± (.43) × 10 ⁻⁹	0.8 ± 0.03	3.8 ± (.72) × 10 ⁻⁶	ND
fMIFL	4.2 ± (.57) × 10 ⁻⁷	0.7 ± 0.1	ND	ND
fMIVTLF	2.4 ± (.24) × 10 ⁻⁸	0.8 ± 0.06	6.0 ± (4.0) × 10 ⁻⁶	0.5 ± 0.2
fMMYALF	2.7 ± (.22) × 10 ⁻⁷	0.7 ± 0.04	ND	ND
fMLFIIK	2.2 ± (.14) × 10 ⁻⁷	0.8 ± 0.03	6.4 ± (2.7) × 10 ⁻⁶	0.9 ± 0.1
MLFIIK	ND	ND	ND	ND
Quin C1	8.5 ± (.52) × 10 ⁻⁶	0.6 ± 0.06	> 1.4 × 10 ⁻⁴	ND
Compound 43	7.8 ± (.28) × 10 ⁻⁶	0.7 ± 0.04	> 6.1 × 10 ⁻⁴	ND

ND, not determined.

Figure 1



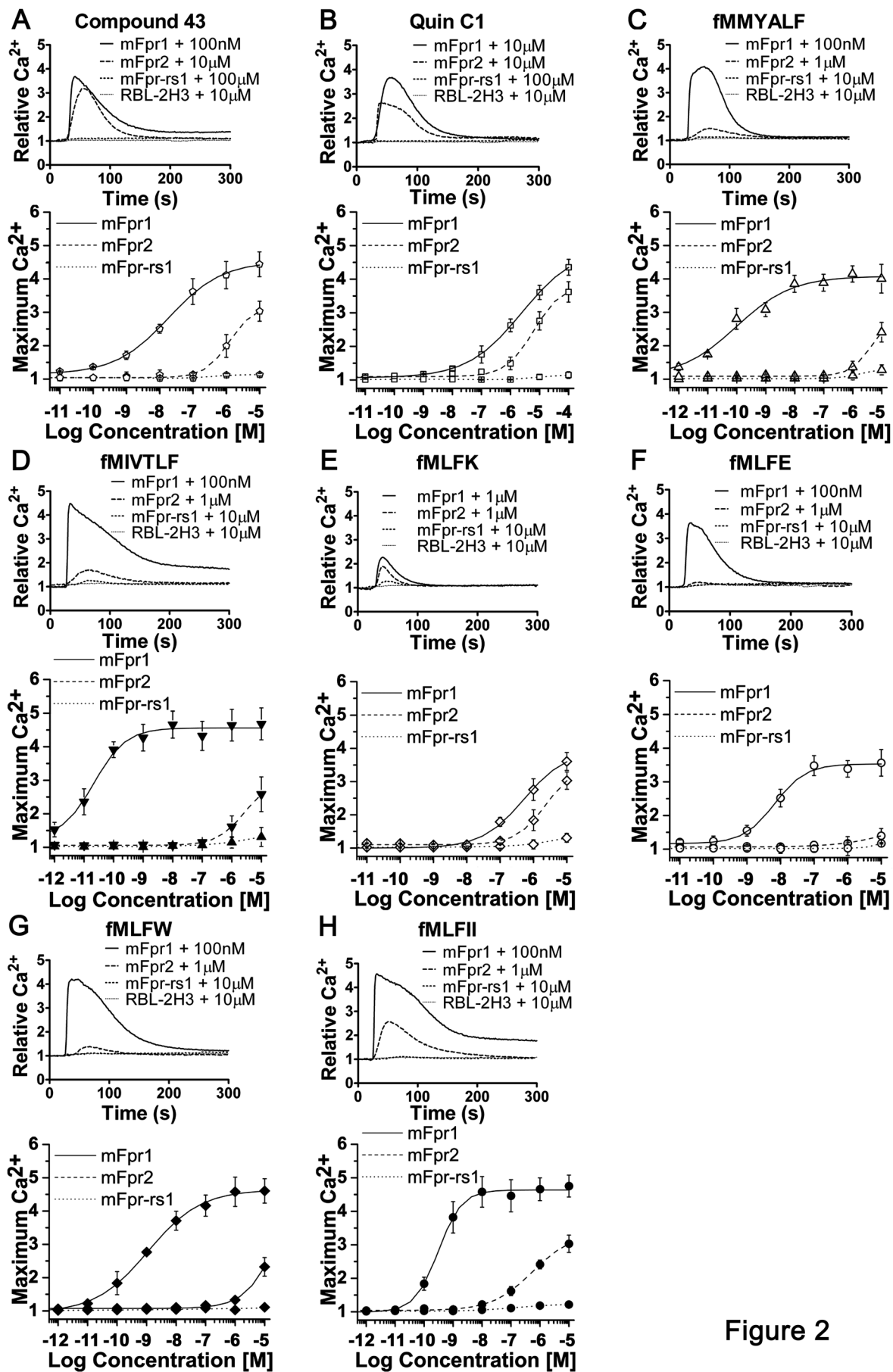


Figure 2

Figure 3

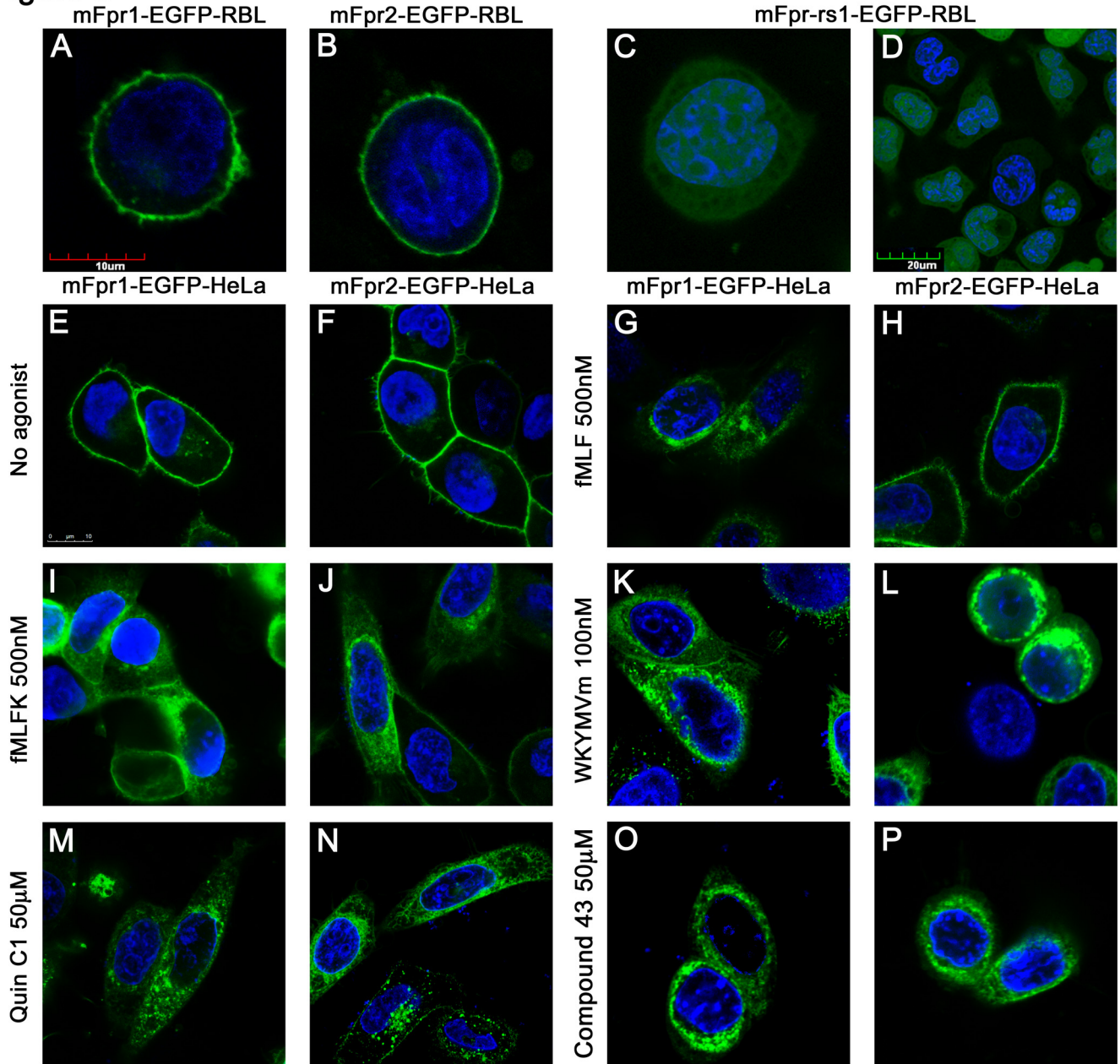


Figure 4

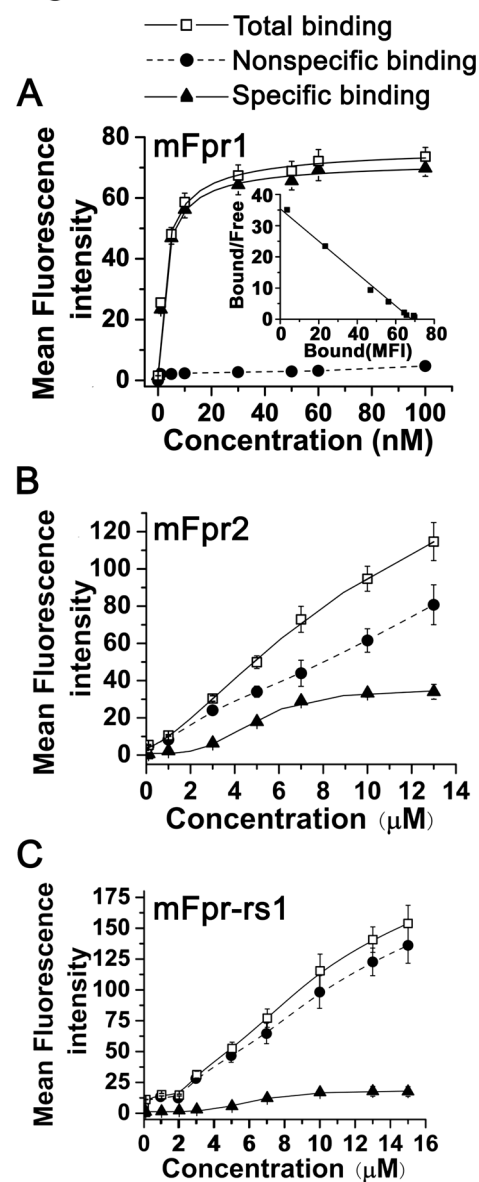


Figure 5

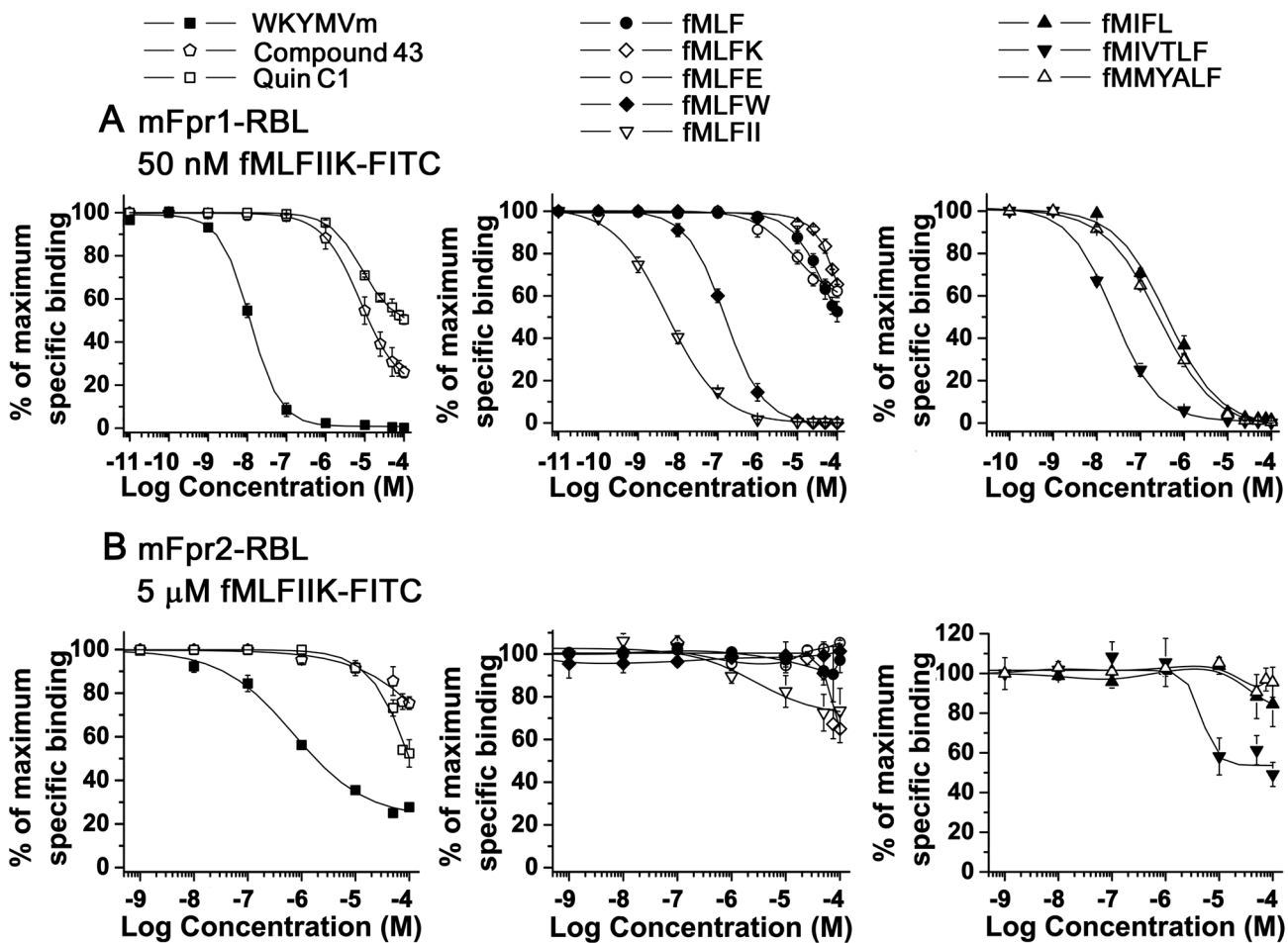


Figure 6

